



## IMPLEMENTATION, VERIFICATION AND ASSESSMENT OF VORTEX CAPTURING CAPABILITIES OF $k-kL$ TURBULENCE MODEL

Erdem DİKBAŞ\* and Özgür Uğraş BARAN\*\*

\* TÜBİTAK SAGE, Aerodynamics Division, 06270 Mamak, Ankara, Turkey  
erdem.dikbas@tubitak.gov.tr, ORCID: 0000-0001-9074-3649

\*\* Middle East Technical University, Mechanical Engineering Department, 06800 Çankaya, Ankara, Turkey  
ubarar@metu.edu.tr, ORCID: 0000-0002-8437-7862

(Geliş Tarihi: 08.10.2021, Kabul Tarihi: 08.04.2022)

**Abstract:** This study presents the first results of a new turbulence model implementation in our compressible finite volume CFD solver. The  $k - kL$  turbulence model is one of the newest two-equation models, and it is based on the ideas of Rotta's two-equation model. Various research groups progressively develop the model, and it is maturing rapidly. Reports suggest that the  $k - kL$  turbulence model provides superior results compared to the other two-equation turbulence models in specific problems. The improved solutions are observed mainly for the flows with high adverse pressure gradients, the blunt-body wakes and jet interactions. We have implemented the  $k - kL$  model (with the standard designation of  $k-kL$ -MEAH2015) in our solver, and we are testing it rigorously. This paper presents our results on standard turbulence test cases: subsonic flat plate and subsonic wall-mounted bump. The results compare well with the reference study previously presented and published by model developers. The design of the  $k - kL$  model prevents excessive production of turbulence and dissipation; hence it preserves vortices significantly better than the other two-equation models. The implemented model is also tested with a transonic fin trailing vortex case to support this statement. Results show that the  $k - kL$  model yields considerably better results than the SST turbulence model in cases including vortices.

**Keywords:** Turbulence models,  $k - kL$  model, Computational Fluid Mechanics

### k-kL TÜRBÜLANS MODELİNİN UYGULAMASI, DOĞRULAMASI VE GİRDAP YAKALAMA YETENEKLERİNİN DEĞERLENDİRİLMESİ

**Özet:** Bu çalışmada, sıkıştırılabilir akış sonlu hacimler çözücümüz üzerinde yeni bir türbülans modeli uygulamasının ilk sonuçları sunulmaktadır.  $k - kL$  türbülans modelinin tarihsel kökleri Rotta'nın iki denklemlilik modeline dayanmaktadır. Birkaç araştırma grubu üzerinde uzun süreli çalışmalar yapmakta ve bu model günümüzde olgunluğa erişmektedir. Geçmiş çalışmalar  $k - kL$  türbülans modelinin diğer iki denklemlilik türbülans modellerine göre bazı alanlarda daha iyi sonuçlar verebildiğini göstermiştir. Özellikler ters basınç gradyanlı akışlar, küt gövde arkası iz akışları ve jet etkileşimleri içeren akışlarda bu olumlu etki gözlemlenmiştir. Bu çalışma kapsamında, standart notasyonda  $k-kL$ -MEAH2015 olarak geçen  $k - kL$  türbülans modeli çözücümüze eklenmiş ve ilk testleri başlamıştır. Ses altı düz levha ve ses altı tümsekli duvar problemleri üzerinde elde edilen sonuçlar sunulmaktadır. Sonuçlar model geliştiricilerinin yayınladığı sonuçlarla örtüşmektedir.  $k - kL$  türbülans modelinin, türbülans denklemlerinin çözümü sırasında aşırı yüksek türbülans üretiminin oluşmasını engelleyerek diğer RANS modellerine göre daha iyi girdaplı akış tahminlerinin yapılmasına yardımcı olması beklenmektedir. Bu sebeple, yeni eklenen model ile ses geçiş hızlarında kanat ucu girdap problem üzerinde testler yapılmış ve Menter'in Shear Stress Transport türbülans modeline göre daha iyi sonuçlar elde edilmiştir.

**Anahtar Kelimeler:** Türbülans modelleri  $k-kL$  modeli, Hesaplamalı Akışkanlar Dinamiği

#### NOMENCLATURE

ARSM Algebraic Reynolds Stress Model

CFD Computational Fluid Dynamics

KSKL  $k\sqrt{kL}$

LES Large Eddy Simulation

NS Navier-Stokes

QCR Quadratic Constitutive Relationship

RANS Reynolds Averaged Navier Stokes

SST Shear Stress Transport

$C$  Model constants

$\delta_{ij}$  Kronecker delta

$k$  turbulent kinetic energy

$L$  Length scale

$t$  time

$x$  Spatial direction

$\mu$  viscosity

$\mu_t$  turbulent viscosity

$\rho$	density
$P$	Turbulent Production term
$u$	$x$ - velocity
$v$	$y$ - velocity
$w$	$z$ - velocity
$\tau_{ij}$	shear stress tensor

## INTRODUCTION

Computational Fluid Dynamics is still a developing area encompassing numerous numerical methods to address different aspects of flow physics. Despite its currently unresolved shortcomings, it is already accepted as a standard design and analysis tool for most engineering flows. CFD methods are based on solving Navier-Stokes equations with various techniques. The discretization of NS equations is often adequate for Laminar flows. Turbulence is one of the essential flow features that conventional CFD methods based on NS discretizations cannot precisely simulate. The main reason for this is the considerable gap between discretization sizes achievable with today's computer capacity and the scales of turbulence. This shortcoming is frequently evaded by applying turbulence models. These models allow replicating turbulence effects into the mean flow on a relatively coarser grid.

Most turbulence models are designed to add turbulence effects by replacing viscosity with an artificial eddy viscosity parameter. The eddy viscosity characterizes the effect of turbulent fluctuations of the flow variables. There are a couple of different turbulence models in the literature with a different number of equations and different complexities. Two-equation models are successfully applied in practical applications. These models rely on the idea that turbulence effects are constituted by two independent scales, obtained from two independent transport equations, as Launder and Spalding (1983) explained.

The  $k - kL$  turbulence model was first developed by Rotta (1951), and since then, there has not been widespread use among the CFD community. This slow adaptation is essentially associated with third-order velocity gradient content contained in the equation set (Menter and Egorov, 2010). A third-order gradient is cumbersome to compute in practice for most finite volume schemes; hence, the application of the solver model did not materialize until recently. However, the historical importance of  $k - kL$  remains. It should be noted that this model constitutes the roots of major families of two-equation models such as  $k - \varepsilon$  and  $k - \omega$ , which are incorporated in many modern CFD solvers (Rodi, 2006). The model has been becoming prevalent in the last few years after the efforts of Menter and Egorov (2010) and Abdol-Hamid (2013, 2015).

The prominent distinguishing feature of Rotta's model is that it employs the turbulent length scale ( $L$ ) concept in the turbulence transport equations. According to this model, the  $kL$  parameter is driven by the third velocity

gradient with the assumption of homogeneous turbulence. On the other hand, Menter and Egorov (2006) suggest that a second-order velocity gradient should drive the turbulent length scale. This approach helps to avoid tedious computation of third derivatives, especially for three-dimensional domains (Menter and Egorov, 2010). The second-order gradient term appears in the von Karman length scale calculation, through which the two turbulence transport equations are coupled. The revision of the length scale discussion leads to the development of  $k - \sqrt{(k)}L$  (KSKL) model, where the preference of  $\sqrt{(k)}L$  parameter is based on historical reasons. KSKL model provides an estimation of local breakups at unstable regions of the flow. This feature may result in an unsteady RANS analysis to exhibit an LES-like behavior where several turbulent scales co-exist in the computed flow field.

The most recent efforts have been made by Abdol-Hamid, while he adapted  $k - kL$  model into NASA solvers. After applying Menter's idea to Rotta's model, he and his colleagues presented and verified the k-kL-MEAH2015 model (Abdol-Hamid, 2016). It is demonstrated that the  $k - kL$  model shows similar or better performance than SST after testing on various problems with different flow regimes. Other variations where quadratic constitutive relationship (QCR) and algebraic Reynolds stress models (ARSM) are incorporated lead to performance improvements (Abdol-Hamid, 2019).

The  $k - kL$  turbulence model is a promising method that incorporates several advantages over standard two-equation models. The main advantage of the model is that the method involves several turbulent length scales. This feature may provide an advantage in simulating flows involving large vortices, whereas other two-equation models produce excessive turbulent stresses, and vortices dissipate rapidly. The fin-vortex may severely affect the missile performance, and it is a challenging task in the missile design process. To address this problem, we have decided to implement the method and assess its characteristics in such flow configurations.

In the current study, the k-kL-MEAH2015 turbulence model is implemented into our in-house flow solver. We used subsonic flat plate and subsonic wall-mounted hump problems as initial validation cases. Test results are presented in comparison with the results of the model developers.

Another critical area that the  $k - kL$  turbulence model is the inclusion of the turbulent length scale parameter,  $L$ . The length scale allows the model to adapt scales of turbulence to local flow characteristics. This feature becomes vital in vortex structures, where the turbulence production is over-predicted in classical models. A compressible-flow fin trailing vortex test case is presented in this study to assess vortex preserving features of the  $k - kL$  turbulence model.

## METHOD

We have implemented the k-kL-MEAH2015 model in our density-based finite volume solver. Our solver applies the HLLC method as the inviscid flux scheme (Toro et al., 1994) and implicit time integration. The software is suited to widely used turbulence models, e.g., Spalart-Allmaras and  $k - \omega$  family. Hybrid RANS-LES models are also supported. Software execution is done fully parallel by MPI libraries. It is possible to input the grids with various element topologies in a wide range of formats. The implementation of the  $k - kL$  model is completed, tests are run in parallel and solutions are compared with the SST type  $k - \omega$  model.

### Theory

The formulation of  $k - kL$  model developed by Abdol-Hamid (2015) is utilized to implement the current study. The governing equations and other relations are presented here for completeness. NASA Langley Turbulence Modeling Resource (Rumsey, 2021) is also utilized for necessary equations.

Scalar transport equations of variables  $k$  and  $kL$  are given as described in k-kL-MEAH2015 in Eqs. 1-2.

$$\frac{\partial(\rho k)}{\partial t} + \frac{\partial(\rho u_j k)}{\partial x_j} = P - C_\mu^{3/4} \rho \frac{k^{5/2}}{(kL)} - 2\mu \frac{k}{d^2} + \frac{\partial}{\partial x_j} \left[ (\mu + \sigma_k \mu_t) \frac{\partial k}{\partial x_j} \right] \quad (1)$$

$$\frac{\partial(\rho(kL))}{\partial t} + \frac{\partial(\rho u_j(kL))}{\partial x_j} = C_{\phi 1} \frac{(kL)}{k} P - C_{\phi 2} \rho k^{3/2} - 6\mu \frac{(kL)}{d^2} f_\phi + \frac{\partial}{\partial x_j} \left[ (\mu + \sigma_\phi \mu_t) \frac{\partial(kL)}{\partial x_j} \right] \quad (2)$$

Production term  $P$ , is computed for both  $k$  and  $kL$  equations using relations in Eqs. 3 through 6. Here, the production term is expressed in terms of the pure strain tensor  $S_{ij}$ . Formulations using the vorticity tensor for the production term are also applicable and can be included as an option in our solver. The production term is limited by the expression given in Eq. 7, as introduced by Abdolhamid.

$$P = \tau_{ij} \frac{\partial u_i}{\partial x_j} \quad (3)$$

$$\tau_{ij} = \mu_t \left( 2S_{ij} - \frac{2}{3} \frac{\partial u_k}{\partial x_k} \delta_{ij} \right) - \frac{2}{3} \rho k \delta_{ij} \quad (4)$$

$$S_{ij} = \frac{1}{2} \left( \frac{\partial u_i}{\partial x_j} + \frac{\partial u_j}{\partial x_i} \right) \quad (5)$$

$$\mu_t = C_\mu^{3/4} \frac{\rho(kL)}{k^{1/2}} \quad (6)$$

$$\min \left( P, 20C_\mu^{3/4} \rho \frac{k^{5/2}}{(kL)} \right) \quad (7)$$

Parameters used in  $kL$ -equation are given in Eq. 8. The second-order gradient of the velocity field,  $U''$ , is utilized in calculating the von Karman length scale,  $L_{vk}$ , which appears in the  $C_{\phi 1}$  function. While implementing the turbulence model into the solver, the gradient of the velocity gradient components is constructed throughout all face and cell centers.

$$C_{\phi 1} = \left[ \zeta_1 - \zeta_{2l} \left( \frac{(kL)}{kL_{vk}} \right)^2 \right] \quad (8a)$$

$$C_{\phi 2} = \zeta_3 \quad (8b)$$

$$C_{\phi 2} = \zeta_3 \quad (8c)$$

$$L_{vk} = \kappa \left| \frac{U'}{U''} \right| \quad (9a)$$

$$U' = \sqrt{2S_{ij}S_{ij}} \quad (9b)$$

$$U'' = \left[ \left( \frac{\partial^2 u}{\partial x^2} + \frac{\partial^2 u}{\partial y^2} + \frac{\partial^2 u}{\partial z^2} \right) + \left( \frac{\partial^2 v}{\partial x^2} + \frac{\partial^2 v}{\partial y^2} + \frac{\partial^2 v}{\partial z^2} \right) + \left( \frac{\partial^2 w}{\partial x^2} + \frac{\partial^2 w}{\partial y^2} + \frac{\partial^2 w}{\partial z^2} \right) \right]^{1/2} \quad (9c)$$

Limiters and constants not given in this paper are used identically with those described in the reference. Boundary conditions for turbulence equations are given in Eqs. 10 and 11 for farfield and wall boundaries, respectively.

$$k_\infty = 9 \times 10^{-9} a_\infty^2 \quad (10a)$$

$$(kL)_\infty = 1.5589 \times 10^{-6} \mu_\infty a_\infty / \rho_\infty \quad (10b)$$

$$k_{wall} = (kL)_{wall} = 0 \quad (11)$$

## VERIFICATION TEST CASES

### Zero pressure gradient flat plate

The test case of the zero-pressure gradient flat plate is described in Figure 1. As perceived from the inlet boundary condition definitions, the test case is specified for compressible flow solvers despite the low-speed free

stream flow ( $M_\infty \sim 0.2$ ). It is one of the AIAA 5th Drag Prediction Workshop (Levy et al., 2014).

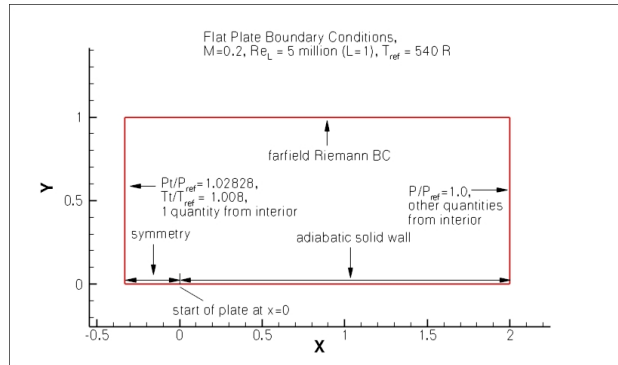


**Figure 1.** Zero pressure gradient flat plate test case description from Turbulence Modeling Resource website (Rumsey, 2021)

In order to keep all the numerical validation test conditions the same, a grid provided on the NASA Turbulence Modeling Resource website is used (Rumsey, 2021). This test case is used among the researchers, and many results are available. In addition to

the NASA Turbulence Modeling Resource website, two AIAA led workshops used this test case, and extensive reports are available (Rumsey, 2015), (Levy, 2014). We will compare our results only with the reference study. Other results with various turbulence models and solvers are available on the website. The grid borrowed for the current study is the structured hexahedral grid with  $2 \times 545 \times 385$  node points on each axis.

### Bump-in-channel

The bump-in-channel test case is described in Figure 2. This test case is specified for compressible flow solvers, similar to the previous case. The bump in the middle triggers flow separation, which is accepted as a challenging test case for RANS models. Indeed, many examples of RANS models are not proven to provide credible results in the case of flow separation. In order to keep all the inputs the same, a grid provided on the NASA Turbulence Modeling Resource website is used (Rumsey, 2021). The grid borrowed for the current study is a structured hexahedral grid with  $2 \times 705 \times 321$  nodes on each axis.

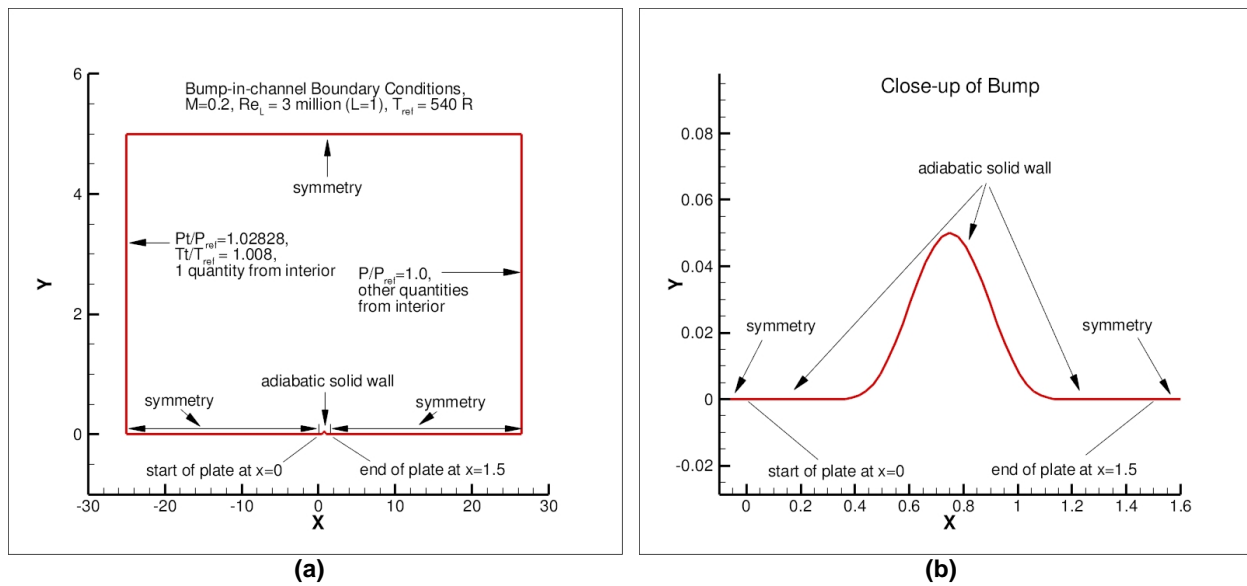


**Figure 2.** Bump-in-channel test case description from Turbulence Modeling Resource website (Rumsey, 2021). (a) domain dimensions, (b) bump details (x-y scales do not match)

## RESULTS

### Verification of the implementation

Verification of the new  $k - kL$  turbulence model implementation is shown on zero pressure gradient flat plate and bump-in-channel test cases. The data set given in the NASA Langley Center Turbulence Modeling Resource webpage (Rumsey, 2021) is used for comparison purposes. Local flow field variables at reference planes and variations of flow quantities within the boundary layer at definite axial stations constitute the basis of the comparisons. Results are presented and discussed in the respective sub-headings.

### Zero-gradient flat plate

The zero pressure gradient flat plate case results have been obtained by utilizing the newly implemented  $k - kL$  turbulence model. Verification of current implementation is done via flow field comparison between new results and those presented by Abdol-Hamid (2016). The computed turbulent viscosity ratio within the boundary layer compares well, as given in Figure 3. Note that the vertical axes are exaggerated for assessment. The current result of the skin-friction coefficient throughout the wall surface mostly coincides with the reference results, except for the foremost region where the gradient of this quantity approaches infinity

(Figure 4.(a)). Velocity,  $k$  and  $kL$  profiles at  $x = 0.97$  station also compare very well to the results of the reference study, as seen in Figure 4. Minor differences in

the free stream turbulence quantities do not significantly affect the flow field prediction within the boundary layer.

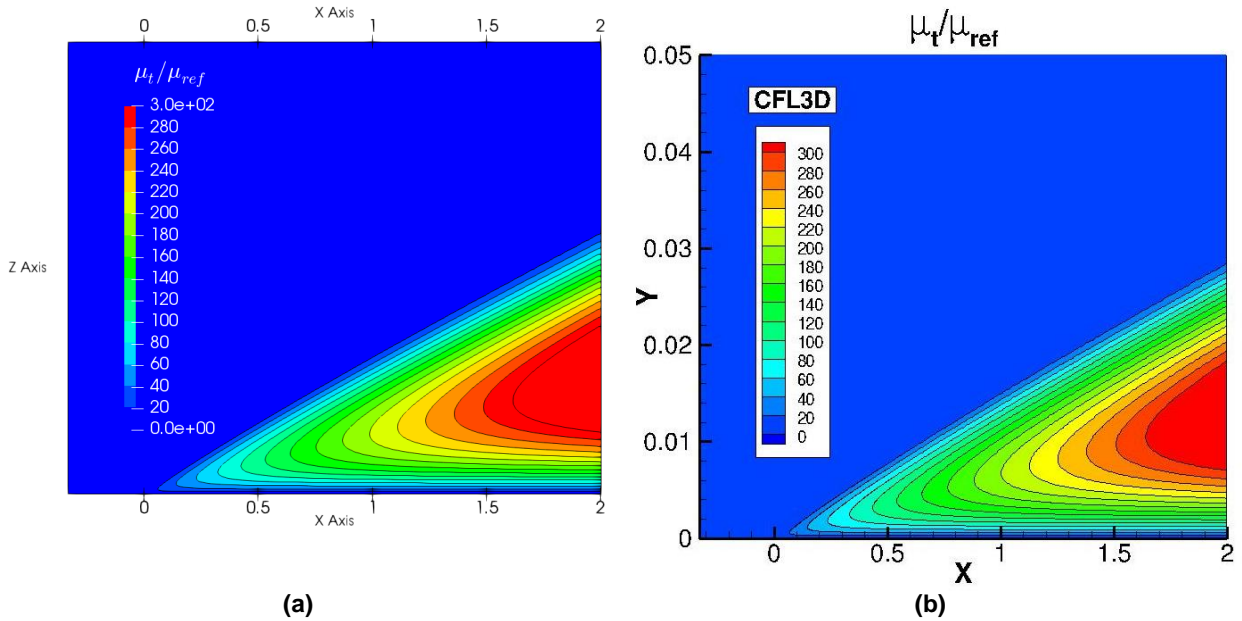


**Figure 3.** Turbulent viscosity ratio within the boundary layer; zero pressure gradient flat plate; (a) – current, (b) – Abdol- Hamid et al.

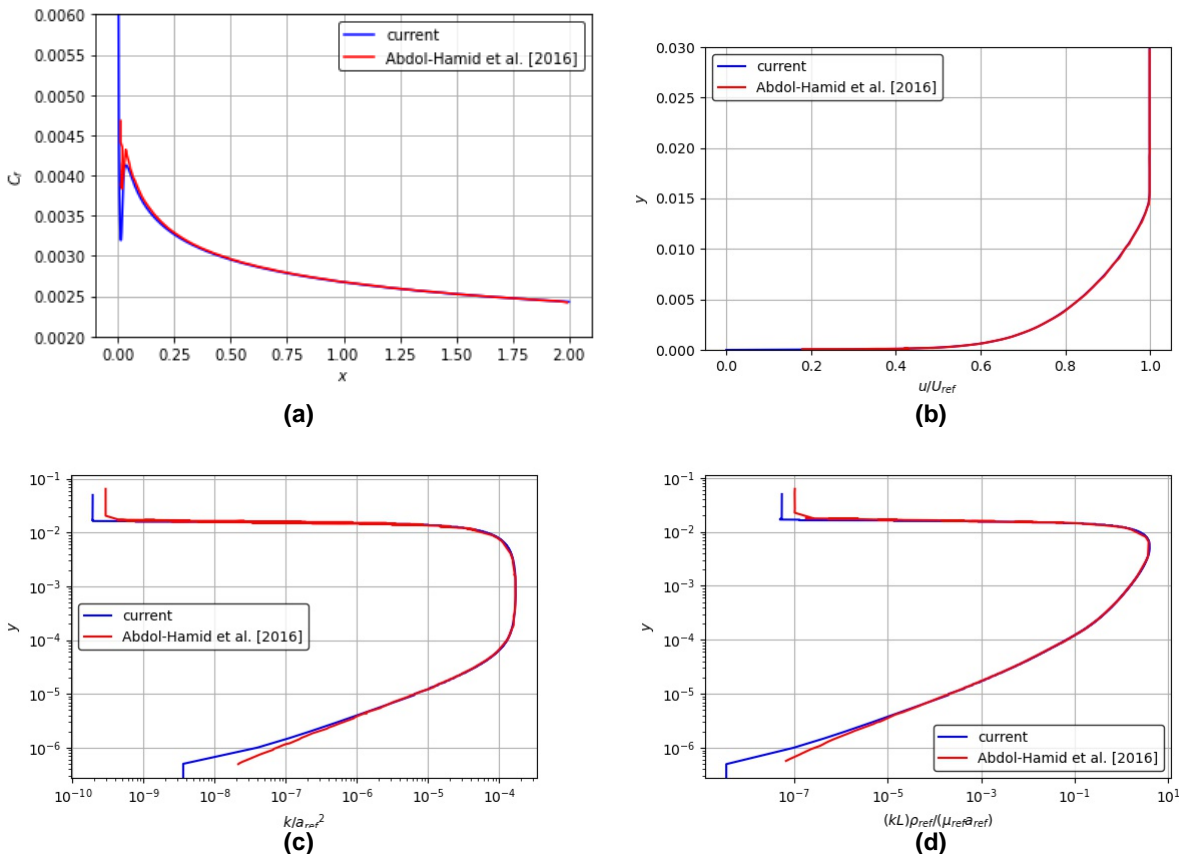


**Figure 4.** Verification of  $k - kL$  implementation; zero pressure gradient flat plate; (a) to (d): skin friction throughout the plate, velocity,  $k$  and  $kL$  profiles at  $x=0.97$

### Bump-in-channel

The results of the bump-in-channel case are, at first, examined qualitatively, as in the previous case. Figure 5

shows turbulent viscosity ratio fields computed by the current implementation of Abdol-Hamid (2021). The contour levels are relatively comparable to a particular location near the downstream end of the bump geometry. After this point, slightly higher turbulent viscosity levels

are predicted by the current implementation. The difference between maximum values of turbulent viscosity is considerably small. It should be noted that this region is exposed to adverse pressure gradient effects. Therefore various factors, e.g., flux scheme and wall distance calculation method, may contribute to this minor difference.

The skin friction coefficient is one of the most significant parameters for this test case. This parameter matches very well with the reference study, as seen in Figure 6. The large skin friction coefficient at the end of the solid wall is observed in most validation results with all turbulence models published on the NASA turbulence

page. Therefore deviations at this location can be ignored. The same plot also shows that pressure distribution is not affected, and it compares well with Abdol-Hamid’s results.

This test case is surprisingly challenging due to the adverse pressure gradient after the bump. The NASA turbulence modeling website provides the boundary layer profile plots at  $x=0.75$  station, i.e., the peak point of the bump geometry. Profile plots in Figure 7 show a good correlation with the reference study, and minor differences in free-stream turbulence are ineffective on the boundary layer flow field, similar to the zero pressure gradient flat plate case.

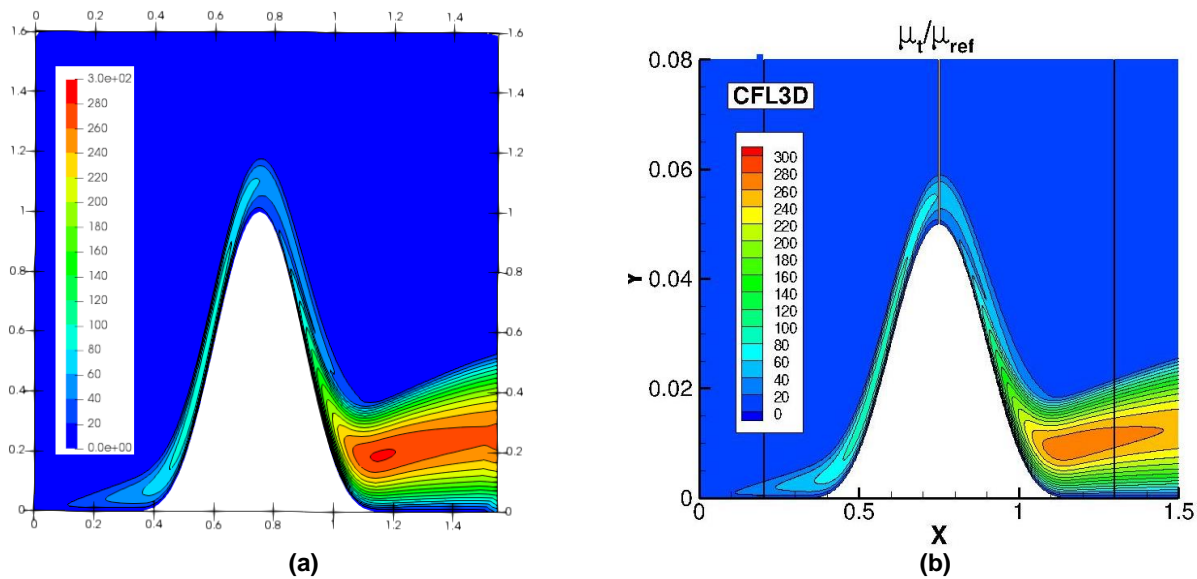


**Figure 5.** Turbulent viscosity ratio within the boundary layer; bump-in-channel; (a) – current, (b) – Abdol-Hamid et al. (2021)

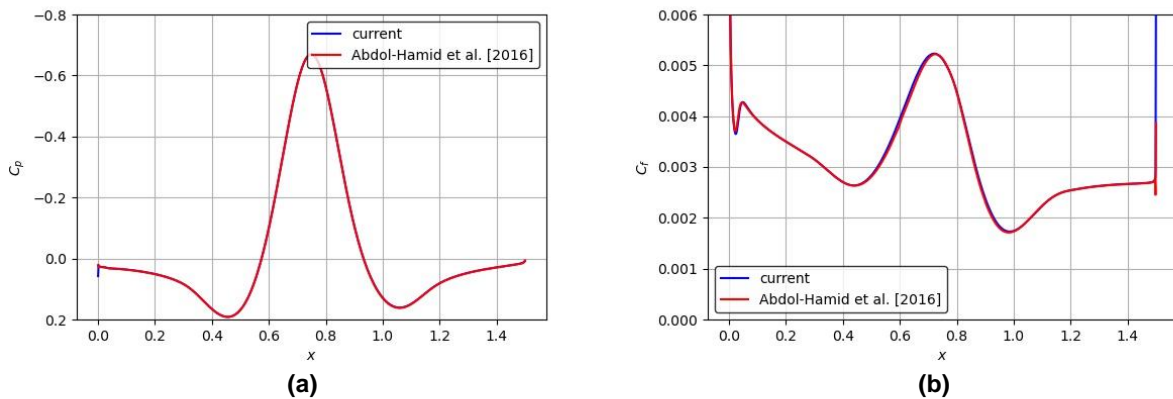


**Figure 6.** Verification of  $k - kL$  implementation; bump-in-channel; pressure (a), and skin friction (b) distributions throughout the plate

## Fin Trailing Vortex

An experimental study in Sandia National Laboratories investigated the isolated fin aerodynamics in upstream vortex flow generated by another fin (Beresh et al., 2009). The test was conducted at various speeds in the Mach number range between 0.50 and 0.80. The angles of both fins were adjustable to have different flow conditions. In this study, local flow measurements were conducted without the existence of the aft fin. The outcomes of this effort are considered helpful for assessing the current study thanks to the measurements of local flow quantities via particle image velocimetry (PIV) technique. Various parameters such as local velocity vector were measured in cross-planes at different locations providing the velocity deficit and vorticity quantities (Beresh et al., 2012).

Initial observations focused on the fin-tip vortex development in the PIV planes located at four cross-sections downstream of the fin at  $x/c = 0.51, 1.18, 2.18, 4.18$ , with  $c$  being root chord length. It was seen that the well-known RANS models could not accurately simulate the vortex core region due to overestimated turbulent viscosity and isotropic turbulence assumption. After  $k - kL$  implementation, the fin trailing vortex case is repeated with this turbulence model. The velocity fields showing the vortex core behavior are depicted in Figure 10. It is clear that the vortex is more intensively preserved up to the most downstream cross-plane when  $k - kL$  turbulence model is utilized. This behavior is much closer to the experimental results at the most downstream cross-plane location.

Turbulent viscosity ratio (TVR) distribution through vortex core explains the better-preserved vortex behavior of the  $k - kL$  turbulence model. Figure 8 explicitly shows the influence of utilizing the  $k - kL$  turbulence model on computed TVR compared to various forms of Shear Stress Transport (SST) turbulence model (Menter, 1994). In this context, we also applied rotation (R) (Dacles-Mariani et al., 1995) and rotation-curvature (RC) (Shur et al., 2000) correction implementations in order to achieve improved results with the SST turbulence model. The function of either correction is to limit the turbulence generation in the vortex core, where the elements of vorticity tensor are dominant over shear stress tensor. The magnitude of TVR computed by  $k - kL$  turbulence model is even below those predicted by the rotational corrections applied on SST.

Tangential velocity profiles through vortex core obtained with all these variants together with those with  $k - kL$  are presented in Figure 9. Tangential velocity distribution in the radial direction is significantly better predicted by  $k - kL$  compared to all SST versions with and without vortex corrections. This is considered another piece of evidence that  $k - kL$  turbulence model better predicts the vortex dynamics compared to SST.

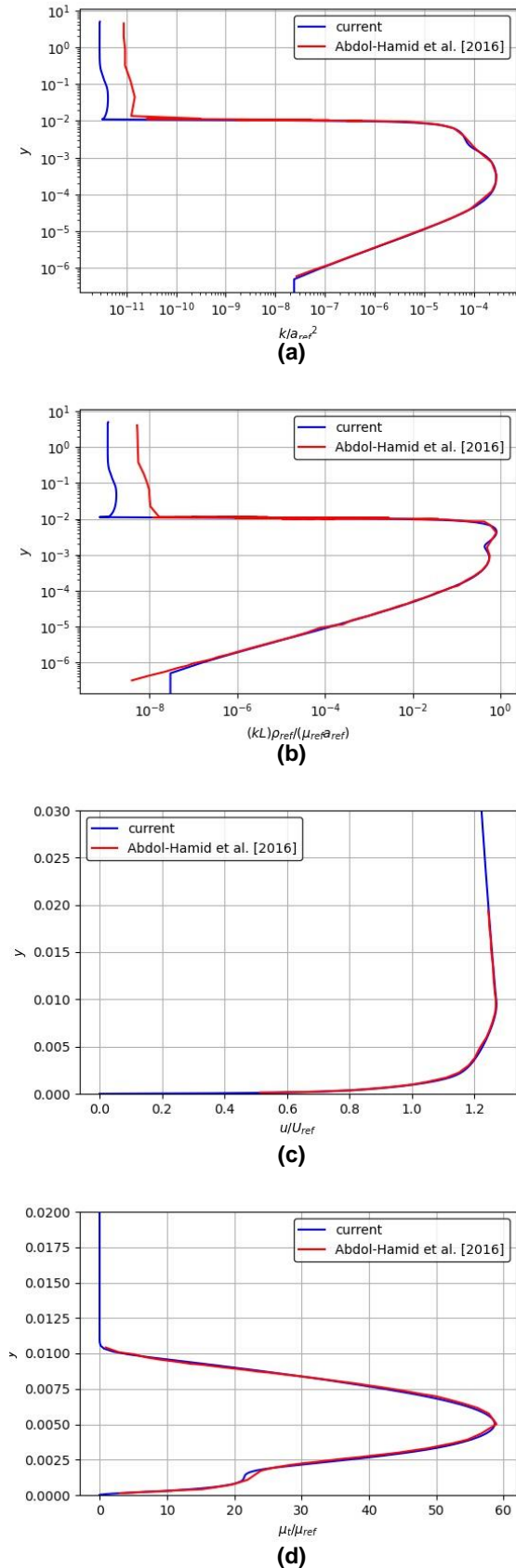


**Figure 7.** Verification of  $k - kL$  implementation; bump-in-channel; (a) to (d):  $k$ ,  $kL$  velocity and turbulent viscosity profiles at bump peak

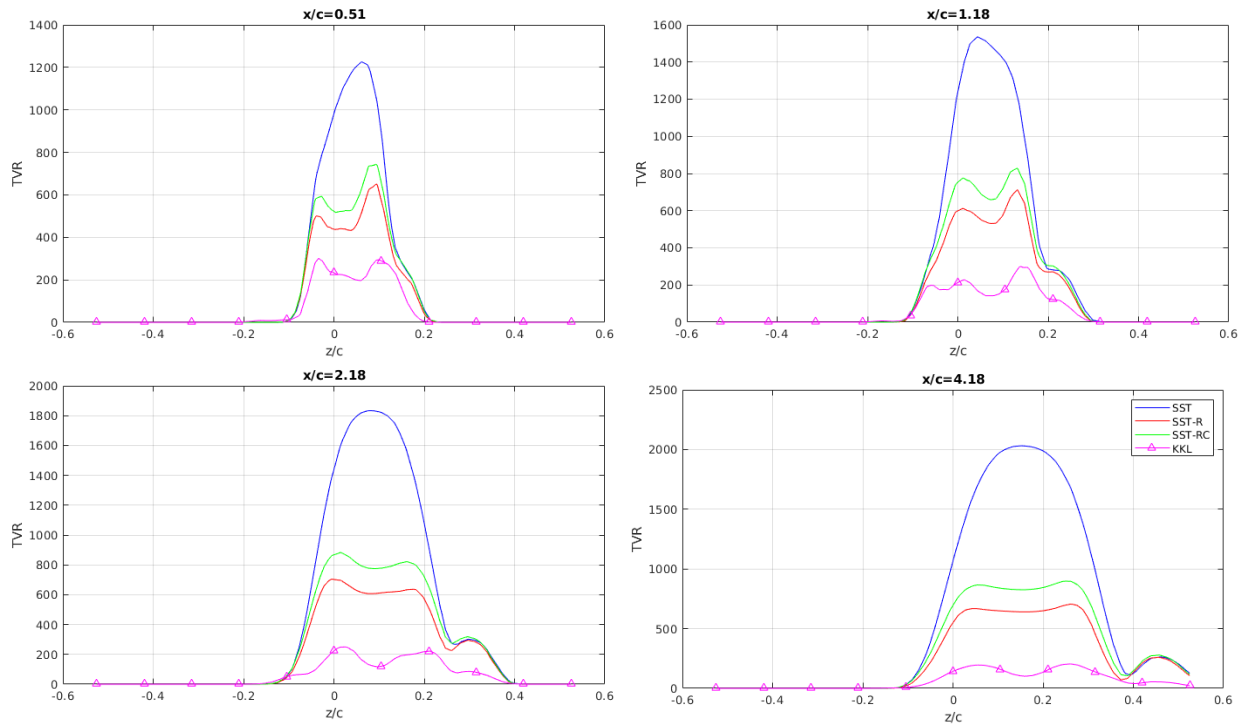


**Figure 8.** Turbulent viscosity ratio distribution through vortex core at different cross-sections; fin trailing vortex

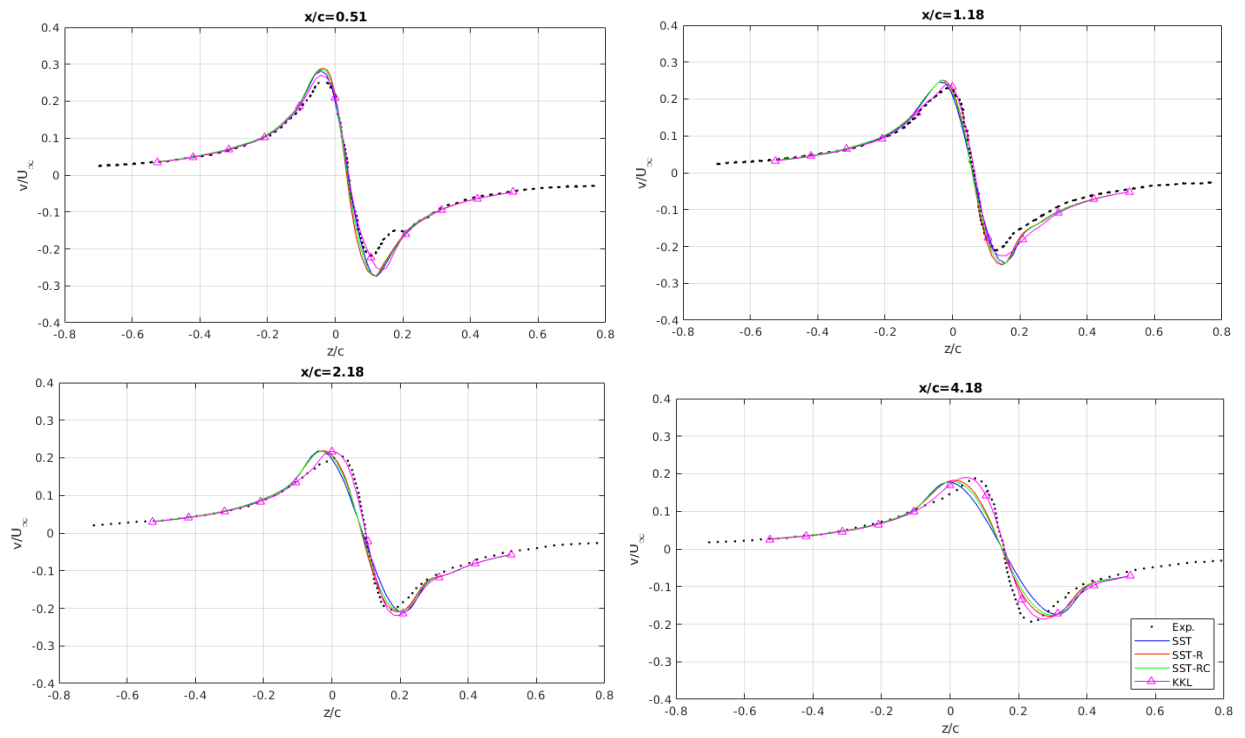


**Figure 9.** Tangential velocity distribution through vortex core at different cross-sections; fin trailing vortex; experimental results from Beresh et al. (2009)

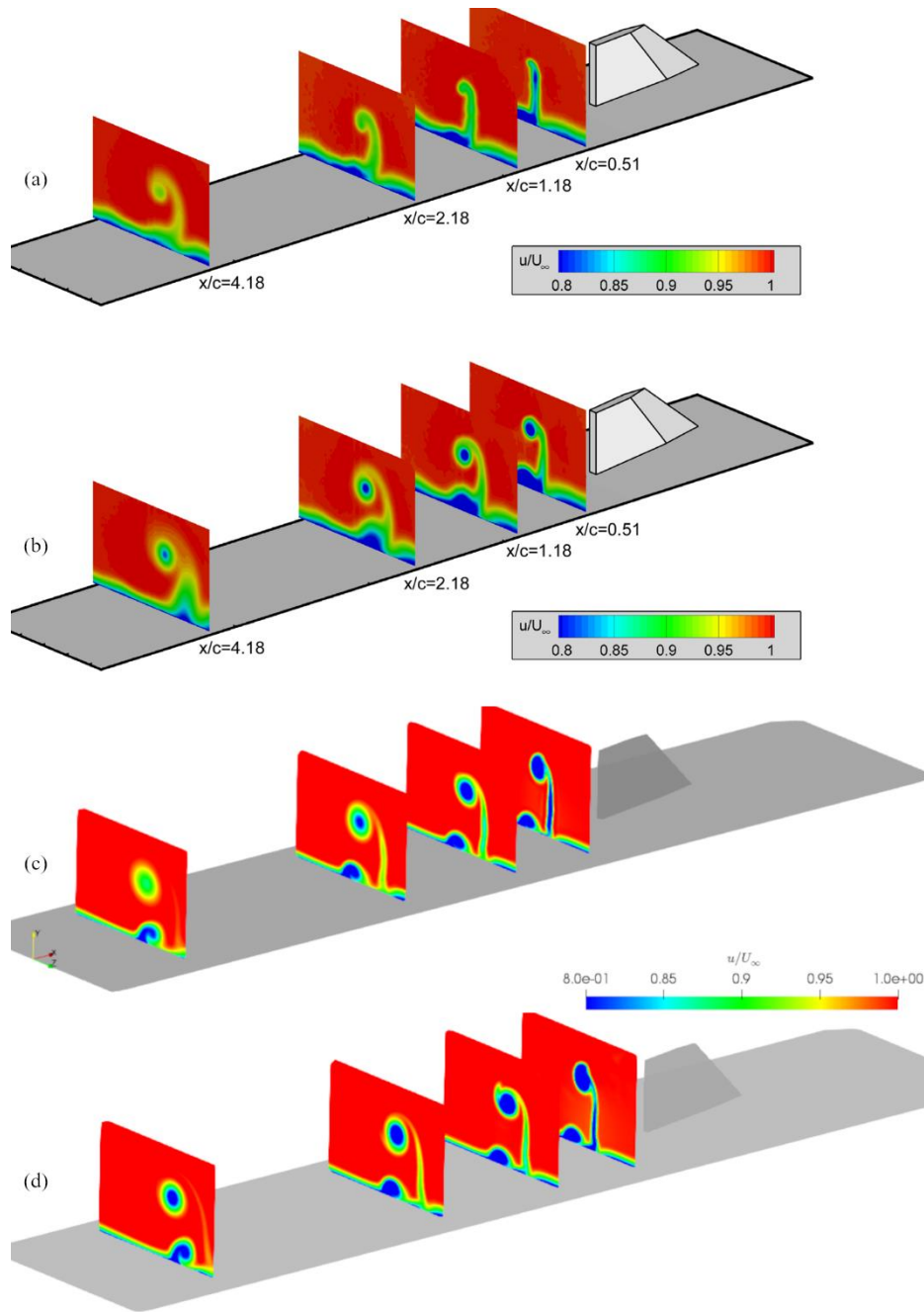


**Figure 10.** Velocity fields at several cross planes downstream of the fin; (a) experiment (Beresh et al., 2009), (b) SST (DeSpirito, 2016), (c) SST (current), (d)  $k - kL$  (current);  $M_\infty=0.80$ ,  $Re=19 \times 10^6 m^{-1}$ ,  $\alpha=10$

## CONCLUSION

In this study, the first results of  $k - kL$  turbulence model implementation in our CFD code are presented. Verification work is held using the data generated by the original developers of the model. The results match with a good margin.

The main aspect of the  $k - kL$  turbulence model is the inclusion of the turbulent length scale  $L$ . The model developers claim that this feature enables the model to resolve different turbulence scales. This capability can be beneficial to resolve separated flows.

The tip vortex generated by the missile fins is an important and challenging topic. These vortices interact with the missile body and other fin-sets and significantly affect missile stability and flight characteristics. Therefore, we have selected a fin-vortex test case to assess the claimed turbulent length-scale resolution feature of the  $k - kL$  model.

The fin trailing-vortex simulation results with  $k - kL$  turbulence model predict the velocity profile at the vortex core considerably better than other commonly used two-equation turbulence models. The vortex strength is preserved better, and significantly less dissipation is observed. The reason for this superior vortex prediction capability at vortices is investigated. It is claimed that the

Turbulence Viscosity Ratio through the vortex core is significantly lower than the other two-equation models.

We are currently conducting further validation tests in a broad spectrum. The following studies will encompass challenging industrial problems with intensive vortex interactions.

## REFERENCES

Abdol-Hamid, K. S., 2013, Assessments of-turbulence model based on Menter's modification to Rotta's two-equation model, AIAA Paper no: 2013-0341.

Abdol-Hamid, K. S., 2015, Assessments of k-kL turbulence model based on Menter's modification to Rotta's Two-equation model. *International Journal of Aerospace Engineering*, 987682.

Abdol-Hamid, K. S., 2019, Development of kL-based linear, nonlinear, and full Reynolds stress turbulence models. *In AIAA Scitech 2019 Forum*, 1878.

Abdol-Hamid, K. S., Carlson, J.-R., and Rumsey, C. L., 2016, Verification and validation of the k-kL turbulence model in FUN3D and CFL3D codes. *In 46th AIAA Fluid Dynamics Conference*, 3941.

Beresh, S.J., Henfling, J.F. and Spillers, R.W., 2009. Planar velocimetry of a fin trailing vortex in subsonic compressible flow. *AIAA Journal*, 47 (7), 1730-1740.

Beresh, S. J., Henfling, J. F., and Spillers, R. W., 2012, Turbulence of a fin trailing vortex in subsonic compressible flow. *AIAA Journal*, 50 (11), 2609–2622.

Dacles-Mariani, J., Zilliac, G. G., Chow, J. S., and Bradshaw, P., 1995, Numerical/experimental study of a wingtip vortex in the near field. *AIAA Journal*, 33(9), 1561–1568.

DeSpirito, J., 2016, CFD validation of interaction of fin trailing vortex with downstream control surface in high subsonic flow. *In 54th AIAA Aerospace Sciences Meeting*, page 1546.

Egorov, Y., Menter, F., Lechner, R., and Cokljat, D., 2010, The scale-adaptive simulation method for unsteady turbulent flow predictions. part 2: Application to complex flows. *Flow, Turbulence and Combustion*, 85 (1), 139–165.

Launder, B. E. and Spalding, D. B., 1983, The numerical computation of turbulent flows. *In Numerical prediction of flow, heat transfer, turbulence and combustion*, 96–116. Elsevier.

Levy, D. W., Laflin, K. R., Tinoco, E. N., Vassberg, J. C., Mani, M., Rider, B., Rumsey, C. L., Wahls, R. A., Morrison, J. H., Brodersen, O. P., et al., 2014, Summary of data from the fifth computational fluid dynamics drag

prediction workshop. *Journal of Aircraft*, 51 (4), 1194–1213.

Menter, F. R. and Egorov, Y., 2006, Revisiting the turbulent scale equation. *IUTAM Symposium on One Hundred Years of Boundary Layer Research*, 279–290, Dordrecht. Springer Netherlands.

Menter, F. R. and Egorov, Y., 2010, The scale-adaptive simulation method for unsteady turbulent flow predictions. Part 1: Theory and model description. *Flow, Turbulence and Combustion*, 85 (1), 113–138.

Rodi, W., 2006, Turbulence modelling for boundary-layer calculations. *In IUTAM Symposium on One Hundred Years of Boundary Layer Research*, 247–256. Springer.

Rotta, J., 1951, Statistische theorie nichthomogener turbulenz. *Zeitschrift für Physik*, 129(6), 547–572.

Rumsey, C. L., 2021, Turbulence modeling resource. <https://turbmodels.larc.nasa.gov>. (Accessed on 04/12/2022)

Rumsey, C.L. and Slotnick, J.P., 2015, Overview and summary of the second AIAA high-lift prediction workshop. *Journal of Aircraft*, 52 (4), 1006-1025.